IS-PORTO 2023 PROCEEDINGS

Proceedings of the 8th International Symposium on DEFORMATION CHARACTERISTICS OF GEOMATERIALS Porto, 3rd - 6th September 2023

Stress–dilatancy behaviour of calcareous sand

Zenon Szypcio[1]

[1]*Bialystok University of Technology, Department of Geotechnics and Structural Mechanics, Wiejska St. 45 A, 15-351 Białystok, Poland*

[#]*Corresponding author: z.szypcio@pb.edu.pl*

ABSTRACT

Calcareous sands are a special geomaterial primarily composed of calcium carbonate or other insoluble carbonate materials susceptible to breakage. Therefore, breakage has a crucial impact on the change of calcareous sand granulation and the shape of individual grains during shear. By analysing some triaxial tests results of some calcareous sands presented in the literature in the light of the Frictional State Concept (FSC), it can be shown that the stress–dilatancy relationship in different shear phases can be approximated with straight lines. These lines are defined by a critical frictional state angle and two material parameters of the FSC. These parameters express the deviation between the stress–dilatancy relationship for tested soil and the stress–dilatancy relationship for isotropic granular material shear deformed without non-coaxiality of the stress tensor and strain increment tensor, breakage, and other effects affecting energy dissipation during shear. It will also be shown that the points representing failure states in the $\eta - D$ plane lie on a straight line with a much higher slope than for silica sands due to the breakage effect. Using the FSC, the stress–dilatancy relationship can be simply described in different shear phases and used to build new elasto-plastic models of calcareous sand in the future.

Keywords: frictional state, stress–dilatancy relationship, calcareous sand

1. Introduction

Calcareous soils refer to the soil formed from the remains of coral, shells, algae, and other marine organisms. In the last few decades, significant attention has been diverted toward the behaviour of calcareous sands due to rapid development in coastal and ocean engineering (Qadimi and Coop 2007, Wang et al. 2011). The behaviours of calcareous sands are significantly different from the quartz sands due to their irregular grain shape, high angularity (Kong et al. 2018, Beemer et al. 2022), low single-particle strength, fragility and high porosity (e.g. Rasouli and Hassanlourad 2017, Coop et al. 2004). The progress of grain crushing during shear, usually quantified by the relative breakage index (Hardin 1985), can be described as a function of the impute work during shear (Hu et al. 2018, Wu et al. 2020). The particle breakage of calcareous sand particles leads to reduced sand dilatancy, smaller peak-state and critical state friction angles (Ueng and Chen 2000, Yu 2019, Wu et al. 2020), as well as the transition and rotation of the critical state line (Zhang and Luo 2020, Liu et al. 2021, Wang et al. 2020).

The stress–dilatancy relationship or plastic potential function are crucial components of every classical elasto-plastic constitutive model developed for soils (Rahimi 2019). The most popular stress–dilatancy relationships were developed theoretically by Rowe (1969) and empirically by Bolton (1969). The general stress–dilatancy relationship for soils was proposed by Szypcio (2016), introducing the natural volumetric plastic strain increment as a linear function of the current volumetric and shear plastic strains increments.

In this paper, the general stress–dilatancy relationship is obtained from the newly formulated *Frictional State Concept* (FSC). The stress–dilatancy behaviour of calcareous sands at different shear stages can be approximated by the linear FSC stress–dilatancy equations defined by the critical frictional state angle (ϕ^o) and two FSC parameters α and β. The dilatant failure state is defined and it is shown that points representing the dilatant failure states in the $\eta - D^p$ plane lie on a straight line independent of the stress path and stress level. It has been shown that for the analysed drained triaxial compression of three calcareous sands can be clearly defined. Therefore, the dilatant failure states can be used to define the critical frictional states. In this paper, this is shown for the $q - p'$ plane.

2. Stress and strain increment tensors

The current state of plastic flow is defined by the effective stress tensor (σ'_{ij}) and plastic strain increment tensor ($\delta\varepsilon^p_{ij}$). Similarly, the reference state of plastic flow is defined by the stress tensor (σ^o_{ij}) and plastic strain increment tensor ($\delta\varepsilon^o_{ij}$).

For isotropic soils, it is convenient to use the principal values of the stress and plastic strain increments. The principal values of the stress and plastic strain increments are (Szypcio 2016)

$$\sigma'_k = p' - \frac{2}{3} q \sin\left\{\theta + \frac{2}{3}(k-2)\pi\right\} \quad (1)$$

$$\sigma^o_k = p^o - \frac{2}{3} q^o \sin\left\{\theta^o + \frac{2}{3}(k-2)\pi\right\} \quad (2)$$

$$\delta\varepsilon^p_k = \frac{1}{3}\delta\varepsilon^p_v - \delta\varepsilon^p_q \sin\left\{\theta_\varepsilon + \frac{2}{3}(k-2)\pi\right\} \quad (3)$$

$$\delta\varepsilon_k^o = \frac{1}{3}\delta\varepsilon_v^o - \delta\varepsilon_q^o \sin\left\{\theta_\varepsilon^o + \frac{2}{3}(k-2)\pi\right\} \quad (4)$$

where k=1, 2, 3

$p' = \frac{1}{3}\sigma'_{kk}$, $q = \left|\sqrt{3J_2}\right|$, $\theta = \frac{1}{3}\sin^{-1}\left\{-\frac{3}{2}\frac{\sqrt{3}J_3}{J_2^{3/2}}\right\}$,

$p^o = \frac{1}{3}\sigma^o_{kk}$, $q^o = \left|\sqrt{3J_2^o}\right|$, $\theta^o = \frac{1}{3}\sin^{-1}\left\{-\frac{3}{2}\frac{\sqrt{3}J_3^o}{J_2^{o\,3/2}}\right\}$,

$\delta\varepsilon_v^p = \delta\varepsilon_{kk}^p$, $\delta\varepsilon_q^p = \left|\sqrt{\frac{4}{3}J_{\varepsilon 2}}\right|$, $\theta_\varepsilon = \frac{1}{3}\sin^{-1}\left\{-\frac{3}{3}\frac{\sqrt{3}J_{\varepsilon 3}}{J_{\varepsilon 2}^{3/2}}\right\}$,

$\delta\varepsilon_v^o = \delta\varepsilon_{kk}^o$, $\delta\varepsilon_q^o = \left|\sqrt{\frac{4}{3}J_{\varepsilon 2}^o}\right|$, $\theta_{\varepsilon 2}^o = \frac{1}{3}\sin^{-1}\left\{-\frac{3}{3}\frac{\sqrt{3}J_{\varepsilon 3}^o}{J_{\varepsilon 2}^{o\,3/2}}\right\}$

and

$J_2 = \frac{1}{2}s_{ij}s_{ij}$, $J_3 = \frac{1}{3}s_{ij}\,s_{jk}\,s_{ki}$, $s_{ij} = \sigma'_{ij} - p'\delta_{ij}$,

$J_2^o = \frac{1}{2}s_{ij}^o s_{ij}^o$, $J_3^o = \frac{1}{3}s_{ij}^o s_{jk}^o\, s_{ki}^o$, $s_{ij}^o = \sigma_{ij}^o - p^o\delta_{ij}$,

$J_{\varepsilon 2} = \frac{1}{2}\delta e_{ij}^p \delta e_{ij}^p$, $J_{\varepsilon 3} = \frac{1}{3}\delta e_{ij}^p \delta e_{jk}^p \delta e_{ki}^p$,

$J_{\varepsilon 2}^o = \frac{1}{2}\delta e_{ij}^o \delta e_{ij}^o$, $J_{\varepsilon 3}^o = \frac{1}{3}\delta e_{ij}^o \delta e_{jk}^o\, \delta e_{ki}^o$,

$\delta e_{ij}^p = \delta\varepsilon_{ij}^p - \frac{1}{3}\delta\varepsilon_v^p\delta_{ij}$, $\delta\varepsilon_{ij}^p = \delta\varepsilon_{ij} - \delta\varepsilon_{ij}^e$,

$\delta e_{ij}^o = \delta\varepsilon_{ij}^o - \frac{1}{3}\delta\varepsilon_v^o\delta_{ij}$.

As traditionally in soil mechanics, positive compression and contraction are assumed. For $-\pi/6 \le \theta \le \pi/6$ and $-\pi/6 \le \theta^o \le \pi/6$ the $\sigma'_1 \ge \sigma'_2 \ge \sigma'_3$, $\sigma_1^o \ge \sigma_2^o \ge \sigma_3^o$ and $\delta\varepsilon_1^p \ge \delta\varepsilon_2^p \ge \delta\varepsilon_3^p$, $\delta\varepsilon_1^o \ge \delta\varepsilon_2^o \ge \delta\varepsilon_3^o$. For triaxial compression $\theta = \theta^o = \pi/6$ and triaxial extension $\theta = \theta^o = -\pi/6$.

The elastic parts of the volumetric and shear strain increments are calculated from equations

$$\delta\varepsilon_v^p = \frac{\kappa}{v}\frac{\delta p'}{p'} \quad (5)$$

$$\delta\varepsilon_q^e = \frac{2}{9}\frac{1+\nu}{1-2\nu}\frac{\kappa}{v}\frac{\delta q}{p'} \quad (6)$$

respectively, where $v = 1 + e$, e-void ratio, ν-Poisson's ratio, κ-parameter of Cam-clay model. In addition, it is assumed that the elastic parts of the volumetric and shear strain increments for the reference state are equal to zero.

3. Critical frictional state

It is assumed that the reference state is the Critical Frictional State (CFS). *CFS* is the state for which the soil can monolithically deform as an isotropic perfectly frictional Mohr–Coulomb material with weightless rigid crushable grains at a constant temperature, water content, Lode angle *(θ),* and constant stress ratio *($q/p' = q^o/p^o = M^o = const.$)* without volume changes induced by shearing *($\delta\varepsilon_v/\delta\varepsilon_q = \delta\varepsilon_v^o/\delta\varepsilon_q^o = 0$).*

For an isotropic Mohr–Coulomb granular material at CFS, the stress ratio is a function only of the Lode angle ($\theta = \theta^o$) and can be expressed by Eq. (7)

$$M^o = M_c^o\, g(\theta^o) \quad (7)$$

where

$$M_c^o = (6\sin\phi^o)/(3 - \sin\phi^o) \quad (8)$$

is the stress ratio for triaxial compression ($\theta^o = \pi/6$) and

$$g(\theta^o) = \frac{3\sin\phi^o}{2\{\sqrt{3}\cos\theta^o - \sin\phi^o\sin\theta^o\}} \quad (9)$$

and ϕ^o is the angle of friction at the CFS. For triaxial extension ($\theta^o = -\pi/6$)

$$M_e^o = (6\sin\phi^o)/(3 + \sin\phi^o) \quad (10)$$

The CFS is represented by a straight line $q^o/p^o = M^o$ in the $q^o - p^o$ plane and a curve $e_c^o = f(p^o, \theta^o)$ in the $e - p^o$ plane (Fig.1).

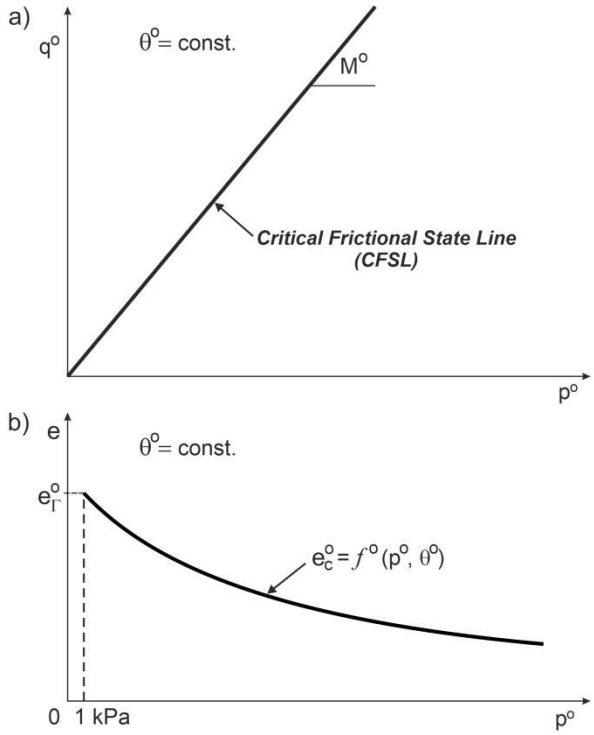

Figure 1. Critical Frictional State in plane: (a) $q^o - p^o$; (b) $e{-}p^o$.

4. The current and appropriate reference state

Assuming the same Lode angles for the current and reference CFS ($\theta = \theta^o$) and shear strain increments ($\delta\varepsilon_q^p = \delta\varepsilon_q^o$) for any shearing stress paths, an appropriate reference CFS can be determined (Fig.2).

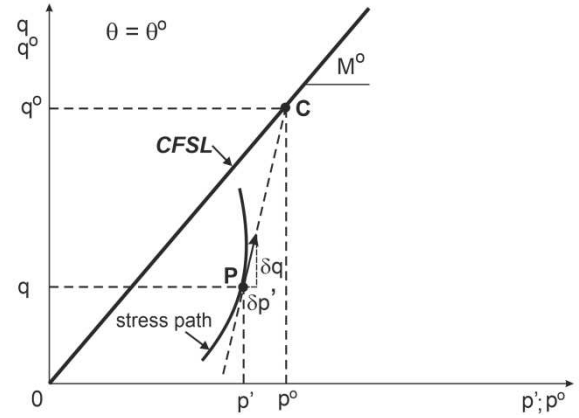

Figure 2. Current and reference states in $q - p'$ plane.

Therefore,

$$(q - q^o)/(p' - p^o) = \delta q/\delta p' \tag{11}$$

or

$$p^o = \{(\eta - \delta q/\delta p')/(M^o - \delta q/\delta p')\}\, p' \tag{12}$$

$$q^o = M^o p^o \tag{13}$$

where $\eta = q/p'$.

5. Energy considerations

Neglecting the elastic part of the stress work increment and the increment of recoverable energy stored in representative elementary volume, the energy equation has the form

$$\delta W^p + \delta W_g = \delta E^p \tag{14}$$

where

$$\delta W^p = p'\delta\varepsilon_v^p + q\delta\varepsilon_q^p \tag{15}$$

for axial symmetry conditions and

$$\delta E^p = \delta E_s + \delta E_b + \delta E_f + \delta E_k + \delta E_a \tag{16}$$

δE_s- increment of energy dissipated at particle contacts, δE_b - increment of energy dissipated in particle bonds, δE_f - increment of particle friction dissipation, δE_κ - increments of kinematic energy of grains, δE_a - additional energy increments not specified above, δW_g - work increment done by gravity force (Wang and Yau 2012). The increment of the energy dissipated in the representative elementary volume can be taken as the sum of the energy dissipated in the reference CFS (δE^o) and the additional part (δE^*)

$$\delta E^p = \delta E^o + \delta E^* \tag{17}$$

where

$$\delta E^o = q^o\delta\varepsilon_q^o = M^o p^o \delta\varepsilon_q^o \tag{18}$$

$$\delta E^* = \delta E^p - \delta E^o. \tag{19}$$

Therefore, the energy equation (14) has the form

$$p'\delta\varepsilon_v^p + q\delta\varepsilon_q^p + \delta W_g - \delta E^* = M^o p^p \delta\varepsilon_q^p \tag{20}$$

In the presented FSC it is assumed that

$$\delta W_g - \delta E^* = p'\{\alpha\, \delta\varepsilon_q^p + (\beta - 1)\delta\varepsilon_v^p\} \tag{21}$$

Combining Eqs. (12), (13), (20) and (21), after some algebra, the general stress–plastic dilatancy relationship is obtained

$$\eta = Q - A\, D^p \tag{22}$$

where

$Q = M^o - \alpha\, A^o$

$A = \beta\, A^o$

$A^o = 1 - M^o(\delta p'/\delta q)$

α and β are new FSC parameters. The values of α and $(\beta - 1)$ represent the energetic "distance" from the current state to the pure frictional state for which $\alpha = 0$ and $\beta = 1$. For the purely frictional state, the change of volume caused by shear strains changes the stresses but does not change the energy dissipated during shear.

$$p'\delta\varepsilon_v^p + q\delta\varepsilon_q^p = M^o p^o \delta\varepsilon_q^p = E^o = const. \tag{23}$$

or

$$\eta = M^o - A^o D^p. \tag{24}$$

In the $\eta - D^p$ plane the straight line defined by Eq. (24) is called the *Frictional State Line* (FSL).

6. Stress–plastic dilatancy behaviour of some calcareous sands

6.1. Dog's Bay sand

The Dog's Bay sand was extensively tested by Coop (1990). Only the results from three drained triaxial compression tests are analysed in this paper: test 11 with constant $p' = 100$ kPa, test H with constant $p' = 3286$ kPa and test L with constant confining pressure $\sigma_c = 4020$ kPa. The experimental results $\sigma_1'/\sigma_3' - \varepsilon_a$ and $\varepsilon_v - \varepsilon_a$ were sectionally approximated by high-degree polynomials, and the relations $\eta - D^p$ were calculated using κ =0.0075 and ν =0.3 (Figs. 3, 4).

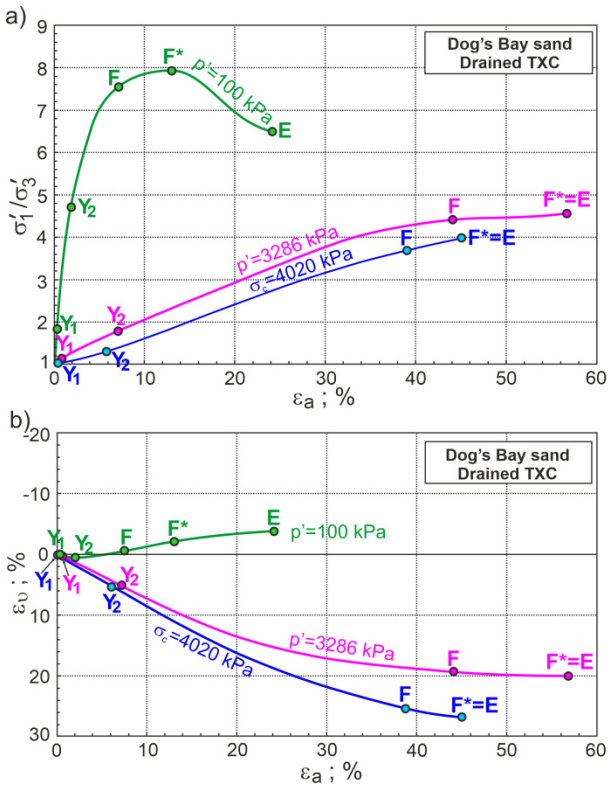

Figure 3. The relationships for drained triaxial compression of Dog's Bay sand: (a) $\sigma_1'/\sigma_3' - \varepsilon_a$; (b) $\varepsilon_v - \varepsilon_a$ (experimental data from Coop 1990).

For each shear test, different phases of shearing can be distinguished from the $\eta - D^p$ relationship (Fig. 4). Point Y_1 represents the end of the elastic phase and the onset of elasto-plastic phases. Further shear deformations cause degradation of the soil structure. The degradation of the soil structure occurs mainly in two elasto-plastic phases. The $\eta - D^p$ curve between points Y_1–Y_2 represents the first phase, and between Y_2–F is the second phase (Fig. 4). The characteristic states, marked with points F in Fig. 3 and 4, are called the *Dilatant Failure State* (DFS).

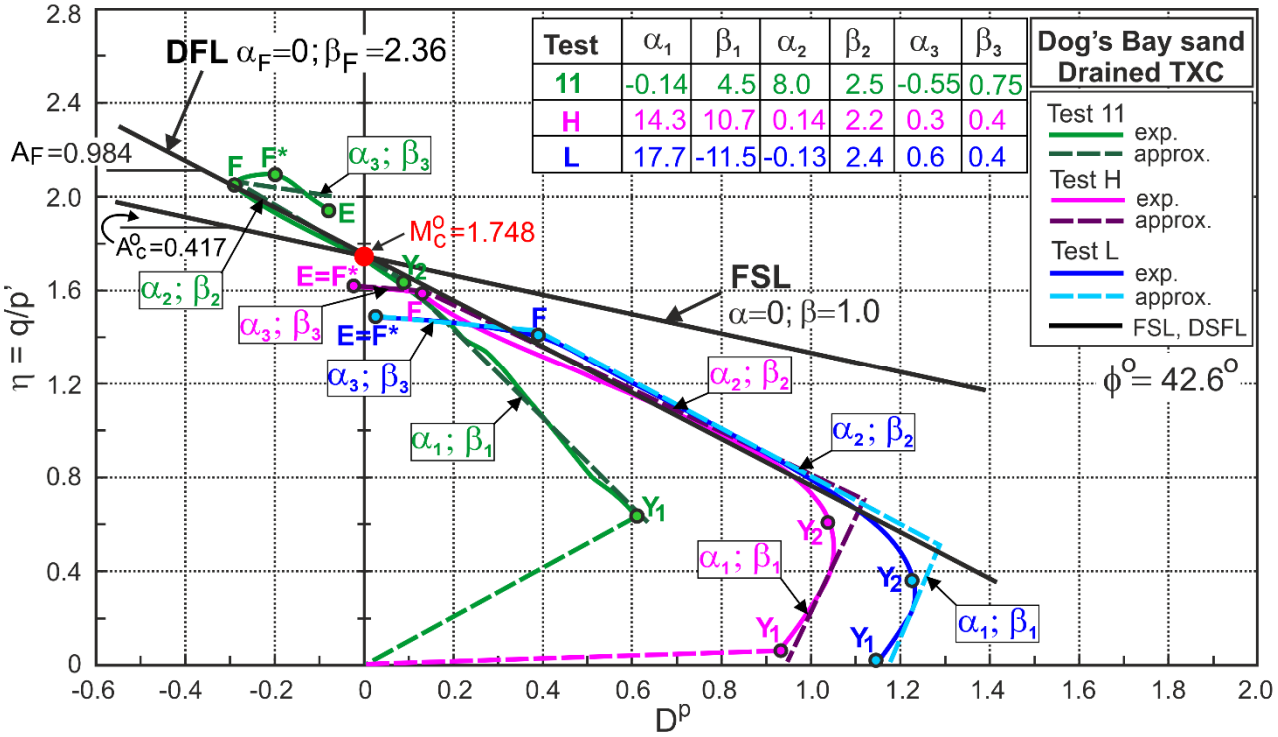

Figure 4. Stress ratio–plastic dilatancy relationships for drained triaxial compression of Dog's Bay sand (experimental data from Coop 1990).

For dilative behaviour, the DFS is at minimum plastic dilatancy (D^p_{min}), and for contractive behaviour at maximum curvature of the $\eta - D^p$ curve (Fig. 4). For Dog's Bay sand, the failure (maximum stress-ratio) states marked as points F* in Fig.4 do not coincide with the DFS. The third phase of elasto-plastic deformation is the post-DFS phase. The E points mark the end of the tests. It can be seen that the distinguishable shear phases in the $\eta - D^p$ planes are not characteristic in the $\sigma_1'/\sigma_3' - \varepsilon_a$ and $\varepsilon_v - \varepsilon_a$ planes (Fig. 3). In all shear phases, the $\eta - D^p$ relationship can be approximated by straight lines determined by Eq. (21) with different values of the α and β parameters (Fig.4). Parameters α_i and β_i fulfilling Eq. (22) are calculated with $A^o = A^o_c = 1$ for p'=constant stress path ($\delta q/\delta p' = \infty$) and $A^o = A^o_c = 1 - M^o_c/3 = 0.417$ for σ_c=constant stress path ($\delta q/\delta p' = 3$). A straight line approximated of the DFS, called the dilatant failure state line (DFSL), is defined by Eq. (22) (Fig. 4) with $\alpha_F = 0$, the slope $A_F = 0.984$, $\beta_F = A_F/A^o_c = 0.984 / 0.417 = 2.358$, intersects the vertical axis at the point with $\eta = M^o_c = 1.748$, which represents the CFS in the $\eta - D^p$ plane ($D^p = 0$). Unlike Dog's Bay sand, for quartz sand without the breakage effect $A_F = A^o_c$ and $\beta_F = 1$ (Szypcio 2016). It can be supposed that A_F greater than A^o_c is a direct effect of grain breakage during shear. It is unexpected that the breakage effect on the DFS of Dog's Bay sand is independent of the stress level and stress path.

In Fig.5 the critical frictional state line with slope $M^o_c = 1.748$ ($\phi^o = 42.6^o$) and the critical state line with slope $M_{cs} = 1.65$ ($\phi_{cs} = 40.3^o$) are shown. The critical frictional state in the e –p' plane is not considered in this paper.

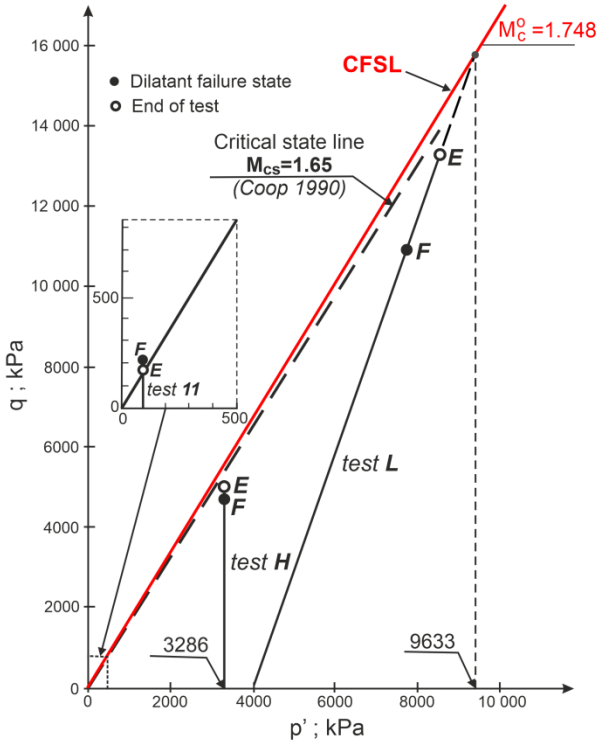

Figure 5. The CFS and critical state for Dog's Bay sand in $q - p'$ plane.

6.2. South China Sea sand

Drained and undrained triaxial compression tests for uniformly graded calcareous sand from the South China Sea were conducted by Wang et al. (2020). To quantify grain crushing development during shear, the various tests were terminated with different axial strains. For

drained triaxial compression, the relative breakage index gradually increases and with axial strain $\varepsilon_a = 20\ \%$ it reaches $B_r = 0.09$ for the confining pressure $\sigma_c = 400$ kPa. For undrained triaxial compression, slightly less grain breakage was observed at the same confining pressure and initial void ratio. Particle breakage makes it easier for the soil grains to change position in relation to each other, which leads to a reduction in the dilation angle, peak friction angle, critical state friction angle and a download shift of the critical state line in the $e - p'$ plane (Wang et al. 2020).

As with Dog's Bay sand, four selected experiments of the drained triaxial compression tests were analysed. The stress–plastic dilatancy relationships obtained from calculations using the elastic parameters $\kappa = 0.0075$ and $\nu = 0.3$ are shown in Fig. 6.

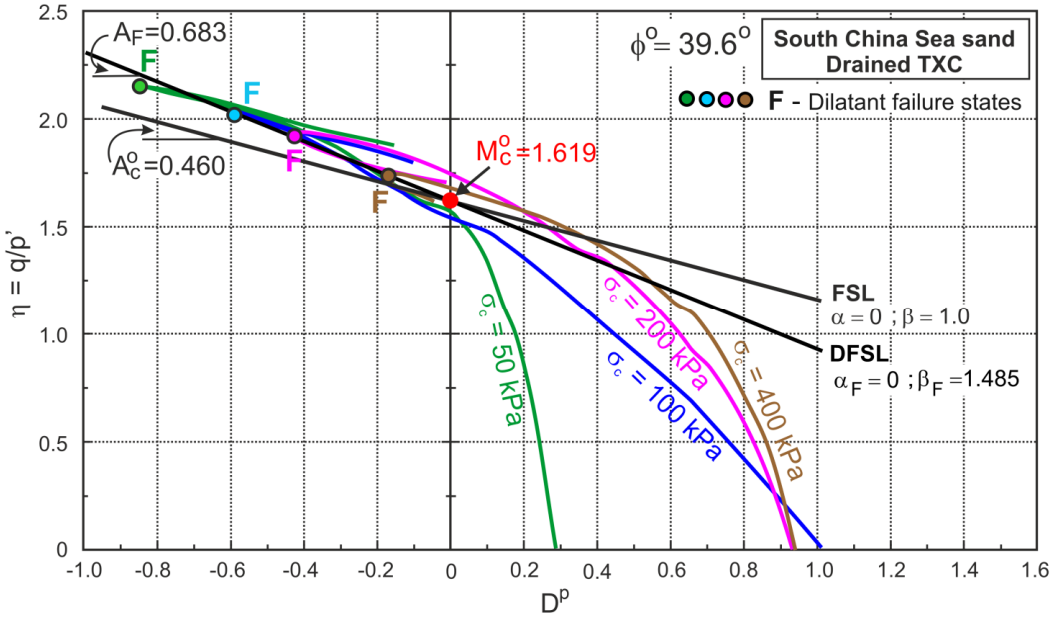

Figure 6. Stress ratio versus plastic dilatancy (experimental data from Wang et al. 2020).

Dilatant failure states only, equal to failure states and denoted as points F, are shown in Fig. 6 for clarity. The straight line DFSL approximating the DFS has a slope $A_F = 0.683$ and intersects vertical axis at $\eta = M_c^o = 1.619$. Therefore, $\phi^o = 39.6°$, $A_c^o = 0.460$, $\alpha_F = 0$ and $\beta_F = 1.485$. Wang at al. (2020) proposed the ratio of major stress (R_{cs}) at critical states (critical state angle) for drained and undrained conditions as a function of relative breakage (Fig. 7).

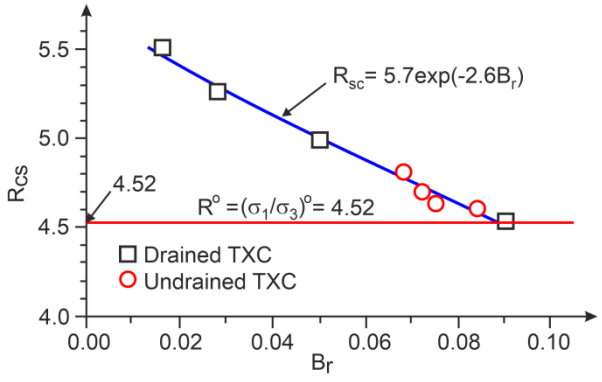

Figure 7. Critical stress ratio and critical frictional stress ratio versus relative breakage (adapted from Wang et al. 2020).

The critical frictional state angle, the ratio of major stress at CFS $R^o = \sigma_1^o/\sigma_3^o = 4.52$ is independent of the relative breakage index (Fig. 7).

6.3. Nansha Island sand

Nansha Island calcareous sand was triaxially compressed using a large-scale triaxial apparatus by Zhang and Luo (2020). The slope of the critical state line in the $q - p'$ plane, the location of the critical state line in the $e - p'$ plane and the plastic dilatancy are expressed as a function of the special breakage parameter and other material parameters. The stress–plastic dilatancy relationships for the selected four tests are shown in Fig. 8.

As for Dog's Bay sand, the DFS can be determined for the dilative and contractive behaviour of this sand during shear (Fig. 8). The straight line DFSL approximating the DFS has a slope $A_F = 0.881$ and intersects the vertical axis at $\eta = M_c^o = 1.515$. Thus the critical frictional state angle $\phi^o = 37.2°$, FSL slope $A_c^o = 0.496$, $\alpha_F = 0$, and $\beta_F = 1.78$. In the model proposed by Zhang and Luo (2020) for this sand, the slope of the critical state line in the $q - p'$ plane without breakage was assumed as $M_{cs} = 1.55$ ($\phi_{cs} = 38.0°$), only 0.8° higher than ϕ^o.

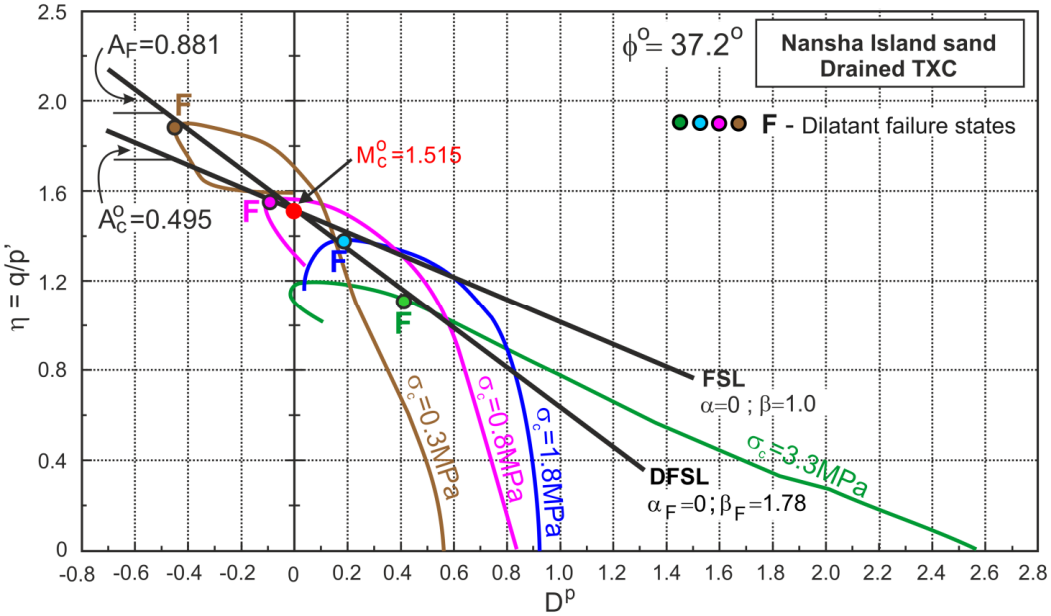

Figure 8. Stress ratio versus plastic dilatancy (experimental data from Zhang and Luo 2020)

7. Conclusions

The general linear stress–plastic dilatancy equation is defined by the critical frictional state angle ϕ^o (M^o) and the two CFS soil parameters (α and β) obtained directly from the energy consideration.

Points representing DFS can be easily identified in the $\eta - D^p$ plane for the dilative and contractive behaviour of soil during shear and can be approximated by the straight DFSL line. The intersects of the DFSL with the vertical axis define the critical frictional state angle (ϕ^o).

The critical frictional state angle is independent of the stress level (breakage) for the analysed calcareous sands.

The DFSL slope for calcareous sands is higher than for quartz sands due to the breakage effect.

For the proposed FSC, the $\eta - D^p$ plane and DFS play a central role.

Acknowledgements

The investigations were conducted at the Bialystok University of Technology (Poland). This research was funded by the Ministry of Science and Education (grant no. WZ/WB-IIL/2/2022).

References

Beemer, R.D., Li, L., Leonti, A., Shaw, J., Fonseca, J., Valova, I., Iskander, M., Pilskaln, CH. Comparison of 2D optical Imaging and 3D Microtomography Shape Measurements of a Coastal Bioclastic Calcareous Sand. Journal of Imaging, 8(3), pp.7272, 2022. http://doi.org/10.3390/jimaging8030072

Bolton, M. D. "The strength and dilatancy of sands", Géotechnique, 36(1), pp. 65-78, 1986. https://doi.org/10.1680/geot.1986.36.1.65

Coop, M. R. "The mechanics of uncemented carbonate sands", Géotechnique, 40(4), pp. 607-626, 1990. https://doi.org/10.1680/geot.1990.40.4.607

Coop, M. R., Sorensen, K. K., Freitas, T. B., and Georgoutsos, G. "Particle breakage during shearing of a carbonate sand", Géotechnique, 54(3), pp. 157-163, 2004. https://doi.org/10.1680/geot.2004.54.3.157

Hardin, B. O. "Crushing of Soil Particles", J Geotech Eng, ASCE, 111(10), pp. 1177-1192, 1985. https://doi.org/10.1061/(ASCE)0733-9410(1985)111:10(1177)

Hu, W., Yin, Z.-Y., Scaringi, G., Dano, C., Hicher, P.-Y. "Relating fragmentation, plastic work and critical state in crushable rock clasts", Eng Geol, 246, pp. 326-336, 2018.https://doi.org/10.1016/j.enggeo.2018.10.012

Kong, D. and Fonseca, J. Quantification of the morphology of shelly carbonate sands using 3Dimages. Géotechnique, 68(3), pp. 249-261, 2016. https://doi.org/10.1680/jgeot.16.p.278

Liu, R., Hou, H., Chen, Y., Ming, P., and Zhu, X. "Elastoplastic constitutive model of coral sand considering particle breakage based on unified hardening parameter", Mar Georesour Geotec 40(6), pp. 655-667, 2022. https://doi.org/10.1080/1064119X.2021.1924321

Qadimi, A., and Coop, M. R. "The Undrained cyclic behaviour of a carbonate sand", Géotechnique, 57(9), pp. 739-750, 2007. https://doi.org/10.1680/geot.2007.57.9.739

Rahimi, M. "Review of Proposed Stress–Dilatancy Relationships and Plastic Potential Functions for Uncemented and Cemented Sands", J Geol Res, 1(2), pp. 19-34, 2019. https://doi.org/10.30564/jgr.v1i2.864

Rasouli, M. R., Hassanlourad, M. "Comparative Study of Carbonate and Quartz Sand Based on Energy Concept", Amirkabir J Civil Eng, 49(1), pp. 89-100, 2017. https://doi.org/10.22060/ceej.2016.592

Rowe, P. W. "The Relation Between Shear Strength of Sands in Triaxial Compression, Plane Strain and Direct Shear". Géotechnique, 19(1), pp. 75–86, 1969.

Szypcio, Z. "Stress-dilatancy for soils. Part I: The frictional state theory", Studia Geotechnica et Mechanica, 38(4), pp. 51–57, 2016. https://doi.org/10.1515/sgem-2016-0030

Ueng, T.-S., Chen, T.-J. "Energy aspects of particle breakage in drained shear of sands", Géotechnique, 50(1), pp. 65-72, 2000. https://doi.org/10.1680/geot.2000.50.1.65

Wang, X.-Z., Jiao, Y.-Y., Wang, R., Hu, M.-J., Meng, Q.-S., Tan, F.-Y."Engineering characteristics of the calcareous

sand in Nansha Islands, South China Sea", Eng Geol,120(1-4), pp. 40-47, 2011. https://doi.org/10.1016/j.enggeo.2011.03.011

Wang, G., Wang, Z., Ye, Q., Wei, X. "Particle Breakage and Deformation Behaviour of Carbonate Sand under Drained and Undrained Triaxial Compression", Int J Geomech, 20(3), p.04020012, 2020. https://doi.org/10.1061/(ASCE)GM.1943-5622.0001601

Wang, J. and Yan, H. "DEM analysis of energy dissipation in crushable soils", Soils Found, 52(4), pp. 644-657, 2012. https://doi.org/10.1016/j.sandf.2012.07.006

Wu, Y., Jie, C., Li, N., Wang, X., Wu, Yi-hang, Guo, Shu-yang. "Experimental study on the mechanical behavior and particle breakage characteristic of hydraulic filled coral sand on a coral reef island in the South China Sea", Rock Soil Mech, 41(10), pp. 3181-3191, 2020. https://doi.org/10.16285/j.rsm.2020.5596

Yu, F. "Influence of Particle Breakage on Behavior of Coral Sands in Triaxial Tests", Int J Geomech, 19(12), p. 04019131, 2019. https://doi.org/10.1061/(ASCE)GM.1943-5622.0001524

Zhang, J. and Luo, M. "Dilatancy and Critical State of Calcareous Sand Incorporating Particle Breakage", Int J Geomech, 20(4), p. 04020030, 2020. https://doi.org/10.1061/(ASCE)GM.1943-5622.0001637